UCD 669.275:539.27

Xiaokun Yuan
College of Materials Science and Engineering, Beijing University of Technology, Beijing, China
yuanxiaokun@bjut.edu.cn

Effect of different binder phases on the Σ2 grain boundary plane distribution in cemented carbides

For WC–6 wt % Co and WC–6 wt % Ni composites, and by using five parameter analysis method as a new approach, the geometric and crystallographic features of carbide/carbide boundaries have been characterized. Two most frequently occurring WC/WC boundaries are 90° twist boundaries about [10-10] (Σ2 boundaries) and 27.8° twist boundaries about [0001] (Σ13a boundaries), the Σ2 boundary populations vary with binder phase types, and carbide crystals are most frequently terminated by (0001) and (10-10) surfaces, such preference does not significantly alter if Σ2 boundaries are partitioned.

Keywords: *Σ2 grain boundary, cemented carbide, binder phase, electron backscattered diffraction, five parameter analysis.*

BACKGROUND

Cemented carbides generally comprise hard carbide phases (e.g. tungsten carbide) embedded in tough metals, or namely binder phases (e.g. cobalt or nickel). The so-called hardmetal alloys have outstanding mechanical properties and accordingly, they are widely used where erosion and abrasion resistance are important [1]. The mechanical properties of hardmetal alloys are strongly influenced by their dense polycrystalline microstructures, which can be described as irregularly shaped and approximately polygonal crystals joined at internal interfaces referred to as grain boundaries or phase boundaries [2]. In turn, characterization of the interfaces distribution is an important issue, which is helpful to understand and thus to improve the properties of such materials. In this field, grain boundary plane crystallography is worthy of special focus, based on the consensus that the mesoscale structure of the grain boundary network could influence a material's integrity and performances [3].

Electron backscattered diffraction (EBSD) is a high capable tool for characterizing the microstructure of engineering materials. The detailed approcaches include crystallographic orientation mapping, phase and texture identification, and grain boundaries revelation. To statistically characterize the grain boundary plane distributions (GBPD) from a batch of EBSD data, there is a recent developed stereological approach named “five parameter analysis (FPA)” method [4]. In this method, the five macroscopic crystallographic parameters are three for lattice misorientation and two for grain boundary plane orientation, thus it can provide a more comprehensive description of the grain boundaries within a polycrystal.

Binder phases are thought to be an essential factor on both structure development during sintering and deformation or fracture evolution during application of

hardmetal alloys [5], however, impact of different binder phases on grain boundary plane crystallography has not been studied. In the current paper, we focus on the most frequently occurring WC/WC coincidence site lattice (CSL) boundary, which can be described as 90 degree rotation about the [10-10] axis and can be abbreviated as Σ2 boundary [6]. Accordingly, the objective of the current work is to use the FPA method to calculate and compare how different binder phases affect the GBPDs of Σ2 boundaries.

MATERIALS AND METHODS

Two cemented carbide samples are selected in this work. Sample 1 (similarly hereinafter) was prepared by sintering in hot isostatic press (sinter-HIP) in a 6 MPa argon atmosphere with a sintering temperature of 1500 °C maintained for 30min. The sample has a cobalt fraction of 6 wt %, an average grain size of about 1 μm, and with no intentional alloying additions. The sample was treated by polishing with diamond abrasive and etching in Murakami's reagent (1 g potassium + 1 g sodium + 10 mL distilled water) for no more than 5 s, and the EBSD measurement was performed by EDAX Hikiari camera incorporated in a FEI Quanta 200 field emission environmental scanning electron microscope (SEM). Sample 2 (similarly hereinafter) was prepared by YLT Hardmetals co, Ltd. The specimen has a nickel fraction of 6 wt % and a mean grain size of approximately 1 μm. The sample was treated by regular metallographic polishing method and did not undergo etching process, and the EBSD analysis was carried out by Oxford Nordlys detector incorporated in a Zeiss Supra 40 field emission gun SEM.

The microtexture and misorientation statistics were represented by the boundary length fraction, and the Brandon criterion was used to determine the fraction of CSL boundaries. The grain shape aspect ratio, which is defined as the length of the minor axis divided by the length of the major axis of the ellipse fitting to a certain grain (and hence ranges from 0 to 1), is used to characterize the shape factor of carbide grains. The ellipse fitted to the grain is calculated by least squares method [7]. The observations needed for the FPA analysis are line segments that are extracted from the orientation maps and are associated with the crystal orientations. Considering the unequivalence of etching process between the specimens, only the line segments correspond to carbide/carbide grain boundaries are selected for further analyze, and segments correspond to carbide/binder and binder/binder interfaces are omitted in this work. Two modes of FPA method are used in this work: (1) the five dimensional calculation considering all five crystallographic parameters is used to calculate the distribution of grain boundary planes of the CSL boundaries; (2) the two dimensional calculation regardless of misorientation is used to calculate the distributions of habit plane of carbide grains averaged over all misorientations. Using the FPA method, the grain boundary plane distribution, $\lambda(\Delta g,n)$, is defined as the relative area of a grain boundary with a misorientation, Δg, and boundary plane normal, n, in units of multiples of a random distribution (MRD). The stereological programs used in this work were developed at Carnegie Mellon University, which contain a stereological procedure coupled with an automated trace analysis step. Further details are given in reference [4].

RESULTS AND DISCUSSION

The microstructures of the two samples are illustrated by the inverse pole figure (IPF) maps in Figs. 1, *a* and *b*, respectively, and the orientation of a certain carbide grain can be determined by the orientation legend for hexagonal symmetries. Both samples exhibit microstructures with randomly oriented prismatic WC grains

embedded in the binder phases. To further analyze the orientation relationship between WC grains, the misorientation angle distribution was calculated. Figure 1, *c* shows the misorientation angle distributions of the two samples. In the chart, the black line represents the misorientation distribution for an ideally random microstructure, while the red and blue lines show the misorientation distributions for the grain boundaries in samples 1 and 2, respectively. It can be seen that the experimental distributions are clearly not random. Two misorientation angle preferences, corresponding to the sharp peaks at 27.8 and 90 degrees, were observed. The peak at 27.8 position corresponds to a relatively high coincidence CSL boundary namely 27.8°/[0001] or Σ13a boundary [6]. There is an even larger deviation from random at the position of 90°, which corresponds to the most frequently occurring carbide/carbide CSL boundaries namely 90°/[10-10] or Σ2 boundary [6]. Moreover, note that sample 2 has higher peaks at both positions than sample 1, indicating that different binder phases remarkably influence the misorientation angle preferences between carbide grain pairs. The role of cobalt during the sintering process of hardmetal alloys has been widely discussed, the structure of the cobalt binder phase can exist in either *fcc* or *hcp* form, and cobalt is described as spreading between WC grains and facilitating rearrangement of the WC into dense clusters, that is, dissolution of small WC particles in the Co takes place with the accompanying

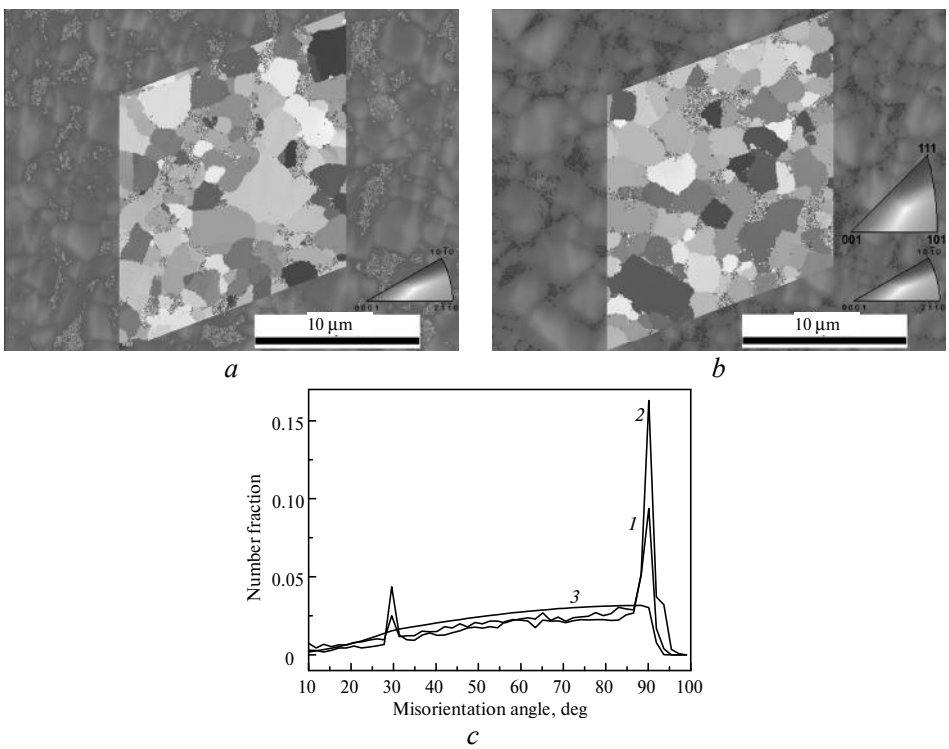

Fig. 1. For sample 1, the IPF map is shown inside the rhombus, with hexagonal orientations legend for tungsten carbide and cobalt; the phase map (red for tungsten carbide and green for cobalt) imposed on image quality (IQ) map is shown outside the rhombus (*a*); for sample 2, the IPF map is shown inside the rhombus, with hexagonal orientations legend for tungsten carbide and cubic orientations legend for nickel; the phase map (red for tungsten carbide and blue for nickel) imposed on IQ map is shown outside the rhombus (*b*); grain boundary populations of carbide crystals and random objects as a function of misorientation angle are illustrated (*c*): *1* – WC–6 wt % Co; *2* – WC–6 wt % Ni; *3* – random.

growth of larger faceted WC particles [1]. On the other hand, although nickel has similar melting point (1455 °C) with cobalt (1450 °C), nickel as binder phase has not been studied in as much detail, despite its potential significance for influencing the structure development during sintering (the detailed approaches are affecting the carbide/binder interface distribution, grain size, or, possible phase content like the *fcc*/*hcp* case of cobalt). Since Fig. 1 had illustrated that different binder phases do affect the carbide/carbide interfaces preference, to further resolve the effect of different binder phases on carbide grains arrangements, we use the technical term namely grain shape aspect ratio that takes both size and shape into account.

In Figs. 2, *a* and *b*, the grain shape ellipses are calculated and imposed on the 2D cross-sections of individual carbide grains, thus each carbide grain has its grain shape aspect ratio value. A very interesting result is repeated in the present work, as illustrated in Fig. 2, *c*, carbide grains have a typical grain shape aspect ratio as about 0.62 (between 0.61 and 0.63 and similarly hereinafter) and this specific value occupies a predominant fraction in both specimens. According to the previous results (for detail please see the supporting information in Fig. 6), grains with grain shape aspect ratios lower than 0.61 have larger grain size and average bulky bar shapes, and can serve as a proxy of later sintering stage in which the anisotropy of the crystal and crystallographic orientations have fully developed. Meantime, grains with grain shape aspect ratios above 0.63 have smaller grain sizes and average equal-axied platelet morphologies, and can serve as a proxy of earlier sintering stage in which the grain shape anisotropy has not been fully developed. Carbide grains with grain shape aspect ratios between 0.61 and 0.63, therefore, correspond

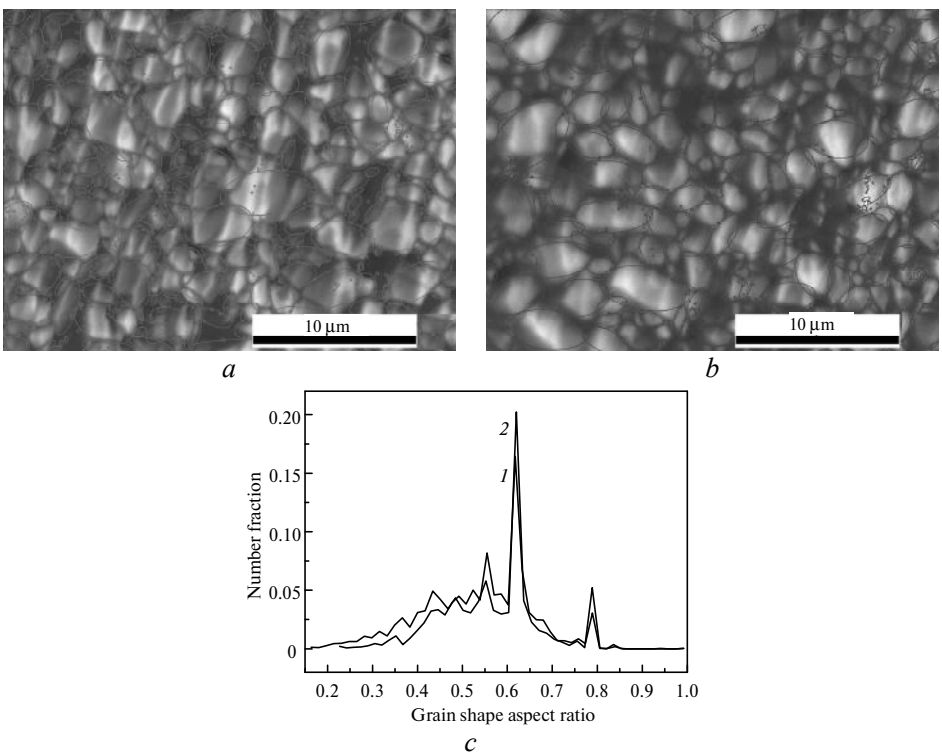

Fig. 2. The microstructures of the samples are illustrated by the IQ maps with grain shape ellipses for sample 1 in (*a*), and for sample 2 in (*b*). Carbide grain populations as a function of grain shape aspect ratio are illustrated in (*c*): *1* – WC–6 wt % Co; *2* – WC–6 wt % Ni.

to medium grain sizes and the shape configuration between bar-like and plate-like, and can therefore represent the intermediate state between the less anisotropic stage and the more anisotropic stage. The deviation of this representative shape factor on two directions may help to determine the size evolution and equilibrium morphology of WC crystals during heating and sintering processes. Further insight into Fig. 2, *c* found that sample 2 has more grains inhibited at the 0.62 stage than sample 1, possibly illustrate that carbide grain growth occurs by dissolution of the small grains and precipitation on the larger is more promoted with nickel binder phase than with cobalt binder phase. To explain this, one can imagine the difference of energy balance or kinetic factors between WC–Co and WC–Ni systems, which could be a possible origin of the crystal shape during growth close to or far from equilibrium shape [8].

The forementioned results demonstrate that different binder phases contribute to either misorientation angle preferences or arrangement features of carbide grains, so it is time to focus on the geometric and crystallographic features of carbide/carbide boundaries with different binder phases. To make the interpretation of CSL boundaries more intuitive, the structures of Σ2 twist boundary and Σ13a twist boundary are illustrated in Fig. 3. The grain boundary plane area distributions considering all five crystallographic parameters for the Σ2 and Σ13a boundaries in the specimens are presented in Fig. 4. In the figure, the boundary plane distribution is the relative areas of different grain boundary planes at certain misorientation with the corresponding rotation axis, and can be determined by referring to the MRD value legend bar. For Σ2 boundaries with misorientation of 90° about [10-10] in both samples, the peak of distribution is at the position of the corresponding misorientation axis, [10-10], marked by an oval, which means the boundary plane is perpendicular to the common rotation axis of the grain pair, thus is a pure twist configuration (see Fig. 3, *a*) where the interface consists of prismatic planes in both grains. The absence of a peak along the great circle perpendicular to the misorientation axes indicates that tilt boundaries where the interface consists of a basal plane in one grain against a prismatic plane in the other are not common.

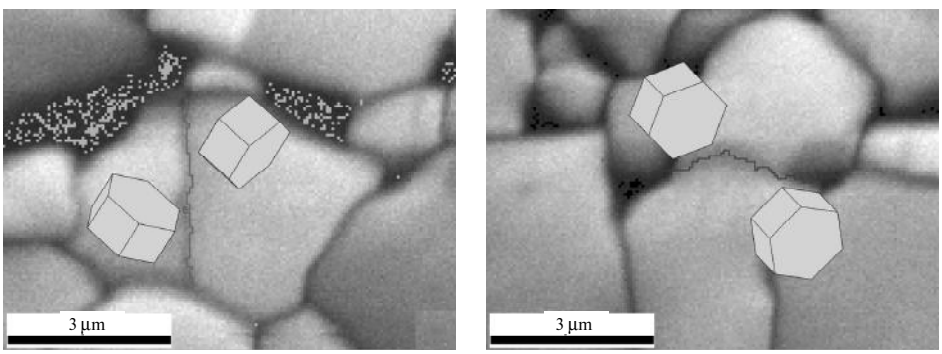

a *b*

Fig. 3. Structures of the Σ2 twist (*a*) and the Σ13a twist (*b*) boundaries. In each figure, two hexagonal unit cells forming the boundary with the IQ map as the background. The Σ2 boundary trace is highlighted in gray (*a*) and the Σ13a boundary trace is highlighted in black (*b*). The orientation relationship of the unit cells is 90°/[10-10] in (*a*), that is, the two lattices rotate 90° to each other along the common [10-10] axis, and have 1/2 of lattice at the coinciding sites on the matched [10-10] prismatic planes. The orientation relationship of the unit cells is 27.8°/[0001] in (*b*), that is, the two lattices rotate 27.8° to each other along the common [0001] axis, and have 1/13 of lattice at the coinciding sites on the matched [0001] basal planes.

The [10-10] misorientation axis brings the necessity of considering the *c*/*a* ratio of tungsten carbide, the ratio value of 0.976 illustrates that Σ2 boundary is actually an "approximate" or "near" CSL boundary [6]. For the samples, the relative area of Σ2 twist boundaries are 36 MRD in sample 1 and 76 MRD in sample 2, indicating that the relative area of Σ2 twist boundaries increases by a factor of 2.1. Σ13a boundaries with misorientation of 27.8° about [0001] in both samples also shown a symmetrical twist configuration (see Fig. 3, *b* around [0001] misorientation axis marked by a hexagon, however, by comparing the maximum at the Σ2 and Σ13a position in both samples, we regard that Σ13a boundaries are less frequent than Σ2 boundaries, and we thus mainly focus the analysis on Σ2 boundaries thereafter.

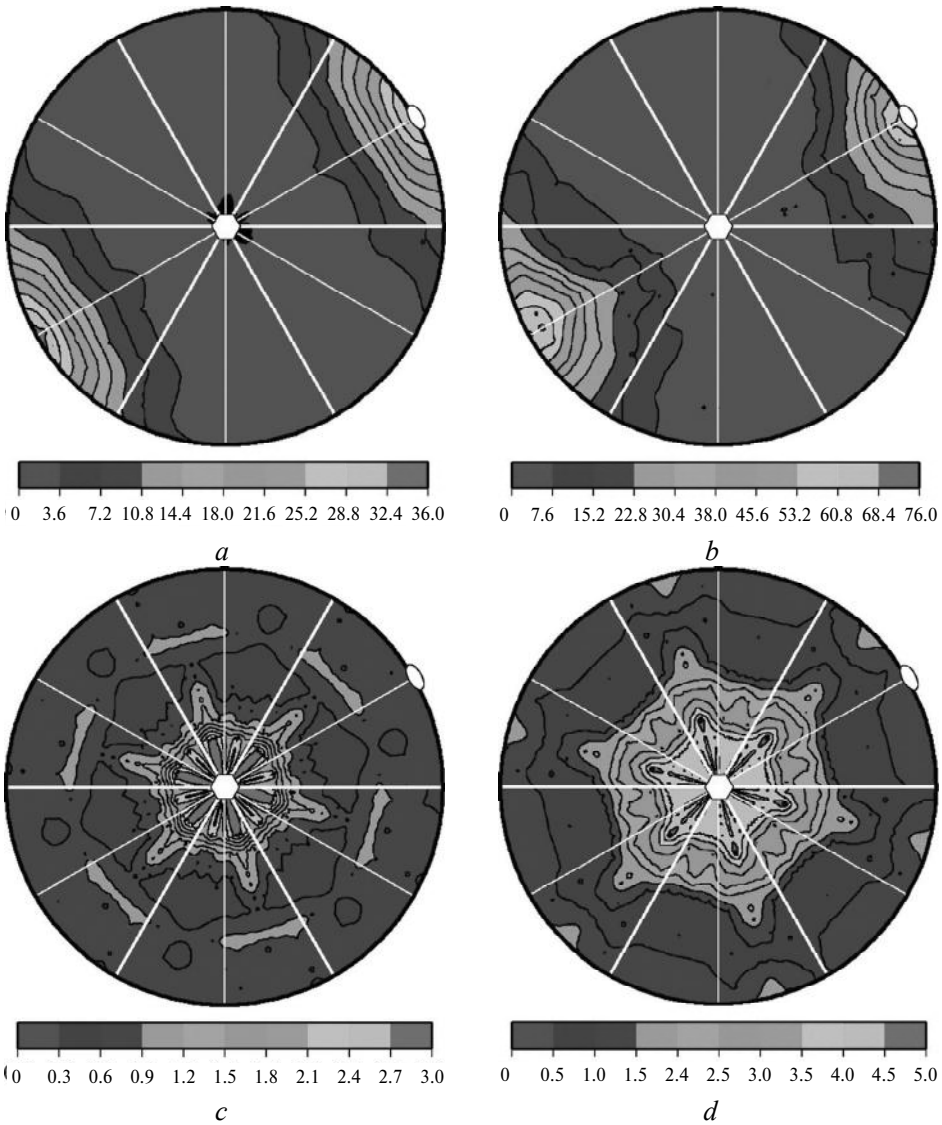

Fig. 4. Grain boundary plane distributions with MRD value legend bar for CSL boundaries in specimens, Σ2, or 90°/[10-10] grain boundaries, in sample 1 (*a*); Σ2 in sample 2 (*b*); Σ13a, or 27.8°/[0001] grain boundaries, in sample 1 (*c*); Σ13a in sample 2 (*d*). The stereograms show distribution peaks at the positions of the [0001] and [10-10] misorientation axes, which are indicated by hexagons and ovals, respectively.

Carbide/carbide grain boundary planes are formed by the intersection of the carbide crystal's habit planes, and by means of two dimensional calculation that regardless of misorientation of FPA method, it had been demonstrated that the average three dimensional crystal habits can be determined by combining the geometric information found in conventional micrographs with crystal orientation data [9]. Moreover, based on the distributions of habit plane of carbide grains averaged over all misorientations, the relative areas of the habit planes can be estimated, and the average shape can thus be defined [10]. Turning to the specimens in this work, the two dimensional calculation results of carbide crystal habit planes are shown in Figs. 5, *a* and *b*. The figures illustrate that the (0001) basal (in the center and

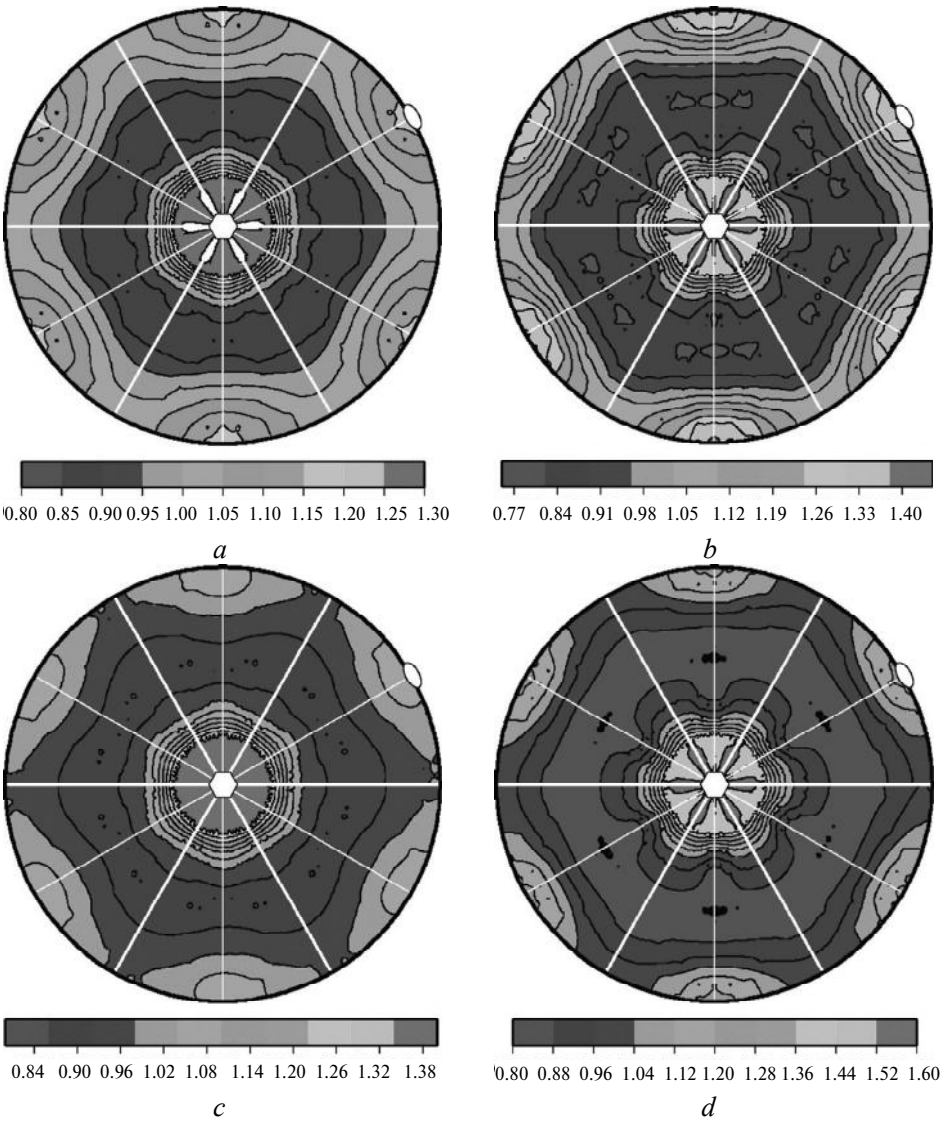

Fig. 5. Grain boundary plane distributions averaged over all misorientations with MRD value legend bar for specimens, with Σ2, in sample 1 (*a*); with Σ2, in sample 2 (*b*); without Σ2, in sample 1 (*c*); without Σ2, in sample 2 (*d*). The stereograms show distribution peaks at the positions of the (0001) basal and (10-10) prismatic orientations, which are indicated by hexagons and ovals, respectively.

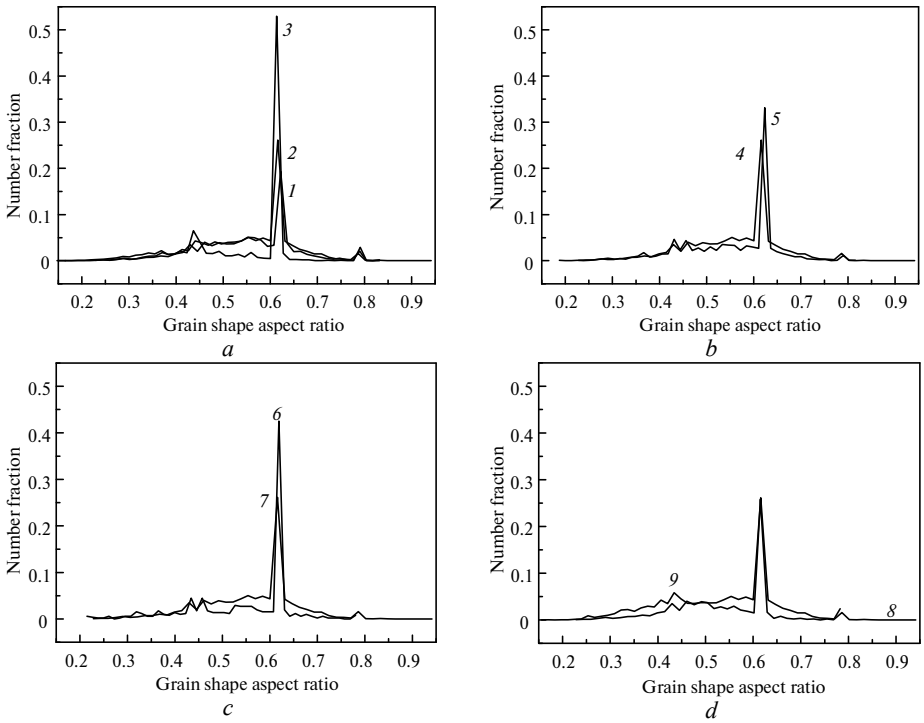

Fig. 6. (supporting information) Carbide grains with grain shape aspect ratio as about 0.62 occupy a predominant number fraction in different cases: concerns the effect of cobalt fraction (*a*); concerns the effect of carbide grain size (*b*); concerns the effect of densification mechanism (*c*); concerns the effect of plastic deformation (*d*): *1* – sample 1 (WC–6 wt % Co); *2* – sample 2 (WC–8 wt % Co); *3* – sample 3 (WC–10 wt % Co); *4* – sample 2 (carbid size 1 μm); *5* – sample 4 (carbid size 2 μm; *6* – sample 2 (sinter-HIPed); *7* – sample 5 (SPSed); *8* – sample 2 (without plastic deformation); *9* – sample 6 (with plastic deformation).

an oval) planes are the most common habit planes, which is consistent with earlier reports [10]. Moreover, for each specimen, the MRD values at basal and prismatic positions differ, indicating the different fractions of the basal and prismatic orientations in the total bounding surfaces. In reference [10], the technical term namely interface area aspect ratio is used to describe the relative basal-to-prism area ratio for a batch of studied carbide grains, and the detailed approach is to calculate the ratio of relative area of (0001) basal facet to the relative area of the (10-10) prism facet, or in other words, the ratios of basal grain boundary area to prismatic grain boundary area, and therefore, the interface area aspect ratio can describe the average shape of the studied carbide grain cluster in a three-dimensional sense. According to this, interface area aspect ratios are 1.08 (1.30/1.20) for sample 1 and 1.00 (1.40/1.40) for sample 2, indicating that the average morphology of carbide grains is affected by different binder phases. The Σ2 boundary is thought to with dense planes [11] and need high work of separation [12], and accordingly, to check the existence of Σ2 boundaries on the average morphologies, the line segments correspond to Σ2 boundaries were sorted out from the rests in both samples, and the outcomes regardless of Σ2 boundaries are shown in Figs. 5, *c* and *d*. The figures illustrate that carbide grains are still most frequently terminated by the (0001) basal and the (10-10) prismatic planes, however, interface area aspect ratios are 1.28 (1.38/1.08) for sample 1 and 1.25 (1.60/1.28) for sample 2 if Σ2 boundaries are neglected. By comparing with the outcomes considering all

line segments, the results indicate that the Σ2 boundaries can make the average morphology of carbide grains more bar-like (with relatively larger prismatic area proportion) other than plate-like (with relatively larger basal area proportion), and such phenomenon occurs no matter cobalt or nickel is as the binder phase. Moreover, this is consistent with Fig. 4 that Σ2 twist boundaries favor (10-10) facets.

SUMMARIES

In summary, the FPA method has been used to compare the grain boundary plane distributions for the Σ2 grain boundaries in cemented carbide samples with different binder phases. The binder phases are shown to affect both misorientation angle preferences and arrangement features of carbide grains (characterized by grain shape aspect ratio), and moreover, the fractional population of Σ2 boundaries. The average morphology of carbide grains (characterized by interface area aspect ratio) various with different binder phases, and Σ2 boundaries can alter this average morphology in both cobalt and nickel cases.

ACKNOWLEDGMENTS

The author acknowledges support from National Natural Science Foundation of China (51471007).

Визначено геометричні і кристалографічні особливості на межі карбідно-карбідних переходів для композитів WC–6 % (за масою) Co і WC–6 % (за масою) методом аналізу п'яти параметрів. Дві межі WC/WC, що найчастіше зустрічаються, – це поворот межі на 90° приблизно [10-10] (межі Σ2) і поворот межі на 27,8° приблизно [0001] (межі Σ13a), сукупності межі Σ2 змінюються в залежності від типів сполучених фаз і кристалів карбіду і найчастіше закінчуються поверхнями (0001) і (10-10), така перевага суттєво не змінюється, якщо межі Σ2 розділені.

***Ключові слова**: межа Σ2, твердий сплав, зв'язуюча фаза, зворотна електронна дифракція, п'ятипараметричний аналіз.*

Определены геометрические и кристаллографические особенности на границах карбидно-карбидных переходов для композитов WC–6% (по массе) Co и WC–6% (по массе) методом анализа пяти параметров. Наиболее часто встречающиеся две границы WC/WC – это поворот границ на 90°, приблизительно [10-10] (границы Σ2), и поворот границ на 27,8°, приблизительно [0001] (границы Σ13a), совокупности границ Σ2 меняются в зависимости от типов соединенных фаз и кристаллов карбида и чаще всего заканчиваются поверхностями (0001) и (10-10), такое предпочтение существенно не меняется, если границы Σ2 разделены.

***Ключевые слова**: граница Σ2, твердый сплав, связывающая фаза, обратная электронная дифракция, пятипараметричний анализ.*

1. Mingard K.P., Roebuck B., Marshall J., Sweetman G. Some aspects of the structure of cobalt and nickel binder phases in hardmetals. *Acta Mater*. 2011. Vol. 59, no. 6. P. 2277–2290.
2. Rohrer G.S., Saylor D.M., Dasher B.E., Adams B.L., Rollett A.D., Wynblatt P. The distribution of internal interfaces in polycrystals. *Int. J. Mater. Res. Adv. Techn*. 2004. Vol. 95, no. 4. P. 197–214.
3. Rohrer G.S. Measuring and interpreting the structure of grain-boundary networks. *J. Am. Ceram. Soc*., 2011, vol. 94, no. 3. P. 633–646.
4. Saylor D.M., Dasher B.S., Adams B.L., Rohrer G.S. Measuring the five-parameter grain boundary distribution from observations of planar sections. *Metall. Mater. Trans. A*. 2004. Vol. 35, no. 7. P. 1981–1989.
5. Roebuck B., Klose P., Mingard K.P. Hardness of hexagonal tungsten carbide crystals as a function of orientation. *Acta Mater*. 2012. vol. 60, no. 17. P. 6131–6143.

6. Hagege S., Nouet G., Delavignette P. Grain boundary analysis in TEM (IV): Coincidence and the associated defect structure in tungsten carbide. *Phys. Status Solidi A*. 1980. Vol. 62, no. 1. P. 97–107.
7. Biggin S., Dingley D.J. A general method for locating the X-ray source point in Kossel diffraction. *J. Appl. Crystallogr*. 1977. Vol. 10, no. 5. P. 376–385.
8. Zhong Y., Zhu H., Shaw L.L., Ramprasad R. The equilibrium morphology of WC particles – A combined ab initio and experimental study. *Acta Mater*. 2011. Vol. 59, no. 9. P. 3748–3757.
9. Saylor D.M., Rohrer G.S. Determining crystal habits from observations of planar sections. *J. Am. Ceram. Soc*. 2002. Vol. 85, no. 11. P. 2799–2804.
10. Kim C.S., Massa T.R., Rohrer G.S. Interface character distributions in WC–Co composites. *J. Am. Ceram. Soc*. 2008. Vol. 91, no. 3. P. 996–1001.
11. Vicens J., Benjdir M., Nouet G., Dubon A., Laval J.Y. Cobalt intergranular segregation in WC–Co composites. *J. Mater. Sci.* 1994. Vol. 29, no. 4. P. 987–994.
12. Christensen M., Wahnstrom G. Co-phase penetration of WC(10-10)/WC(10-10) grain boundaries from first principles. *Phys. Rev. B*. 2003. Vol. 67, no. 11, art. 115415/1-11.

Received 18.04.18
Revised 29.05.18
Accepted 14.06.18